Magic-angle spinning NMR spectral editing of polysaccharides in whole cells using the DREAM scheme

Loic Delcourte, Mélanie Berbon, Marion Rodriguez, Kamalraj Subban, Alons Lends, Axelle Grélard, Estelle Morvan, Birgit Habenstein, Sven Saupe, Laurence Delhaes, et al.

Methods 230 (2024) 59–67

Contents lists available at ScienceDirect

Methods

journal homepage: www.elsevier.com/locate/ymeth

Magic-angle spinning NMR spectral editing of polysaccharides in whole cells using the DREAM scheme

Loic Delcourte [a], Mélanie Berbon [a], Marion Rodriguez [b], Kamalraj Subban [c], Alons Lends [a], Axelle Grélard [a], Estelle Morvan [d], Birgit Habenstein [a], Sven J. Saupe [e], Laurence Delhaes [b,f], Vishukumar Aimanianda [g], Asen Daskalov [c,h,*], Antoine Loquet [a,*]

[a] Univ. Bordeaux, CNRS, Bordeaux INP, CBMN, UMR 5248, IECB, Pessac, France
[b] CNR des Aspergilloses Chroniques, Mycology-Parasitology Department, CHU Bordeaux, Bordeaux 33000, France
[c] ImmunoConcEpT, CNRS, UMR 5164, University of Bordeaux, Bordeaux, France
[d] Univ. Bordeaux, CNRS, Inserm, IECB, UAR3033, US01, Pessac, France
[e] CNRS, Université de Bordeaux, IBGC, UMR 5095, Bordeaux, France
[f] Centre de Recherche Cardio-Thoracique de Bordeaux, Inserm UMR 1045, Univ Bordeaux, Bordeaux 33000, France
[g] Institut Pasteur, Université Paris Cité, Immunobiology of Aspergillus, Mycology Department, Paris, France
[h] State Key Laboratory for Managing Biotic and Chemical Treats to the Quality and Safety of Agro-products, Institute of Plant Protection and Microbiology, Zhejiang Academy of Agricultural Sciences, Hangzhou, China

A B S T R A C T

Most bacterial, plant and fungal cells possess at their surface a protective layer called the cell wall, conferring strength, plasticity and rigidity to withstand the osmotic pressure. This molecular barrier is crucial for pathogenic microorganisms, as it protects the cell from the local environment and often constitutes the first structural component encountered in the host-pathogen interaction. In pathogenic molds and yeasts, the cell wall constitutes the main target for the development of clinically-relevant antifungal drugs. In the past decade, solid-state NMR has emerged as a powerful analytical technique to investigate the molecular organization of microbial cell walls in the context of intact cells. ^{13}C NMR chemical shift is an exquisite source of information to identify the polysaccharides present in the cell wall, and two-dimensional ^{13}C–^{13}C correlation experiments provide an efficient tool to rapidly access the polysaccharide composition in whole cells. Here we investigate the use of the adiabatic DREAM (for dipolar recoupling enhancement through amplitude modulation) recoupling scheme to improve solid-state NMR analysis of polysaccharides in intact cells. We demonstrate the advantages of two-dimensional ^{13}C–^{13}C experiments using the DREAM recoupling scheme. We report the spectral editing of polysaccharide signals by varying the radio-frequency carrier position. We provide practical considerations for the implementation of DREAM experiments to characterize polysaccharides in whole cells. We demonstrate the approach on intact fungal cells of *Neurospora crassa* and *Aspergillus fumigatus*, a model and a pathogenic filamentous fungus, respectively. The approach could be envisioned to efficiently reduce the spectral crowding of more complex cell surfaces, such as cell wall and peptidoglycan in bacteria.

1. Introduction

Most microbes including bacteria, yeasts, filamentous fungi and pathogenic molds present an elaborated structural organelle at their surface called the cell wall (CW). The CW is found outside of the lipidic plasma membrane and helps the cell to withstand the osmotic pressure. As such, the CW possesses an intrinsic rigidity allowing the cell to maintain a mechanical integrity and avoid unwanted cell lysis [1]. This mechanical strength is crucial for microbe survival when cells are exposed to external environmental stress such as fluctuating chemical/pH conditions or competing microorganisms or viruses (e.g. bacteriophages for bacteria). Moreover, pathogenic microbes might directly encounter host immune defenses during the infection process, and the CW often constitutes the first component recognized by host receptors [2,3]. While conferring the required cell surface rigidity, the fungal CW possess a complex structure allowing some degree of dynamics, e.g. to undergo morphologically remodeling during cell growth [4,5] or to allow the diffusion of small molecules or extracellular vesicles [6]. Due to its critical role in survival and proliferation of pathogenic microbes, the CW constitutes a target of choice for the development of antimicrobial compounds. Because microbial CW biomolecules are absent in humans, the development of antibiotics and/or antifungals

* Corresponding authors at: ImmunoConcEpT, CNRS, UMR 5164, University of Bordeaux, Bordeaux, France and CBMN, CNRS, UMR5248, University of Bordeaux, France.
E-mail addresses: asen.daskalov@u-bordeaux.fr (A. Daskalov), a.loquet@iecb.u-bordeaux.fr (A. Loquet).

https://doi.org/10.1016/j.ymeth.2024.07.003
Received 13 June 2024; Received in revised form 12 July 2024; Accepted 15 July 2024
Available online 22 July 2024

targeting the biosynthesis of CW components remains one of the most promising route to fight the current global antimicrobial resistance [7,8].

Considering filamentous and yeast fungal pathogens, the CW presents a typical molecular composition, mainly dominated by glucans, chitins and glycoproteins [9]. Their complex organization into a semi-rigid cell wall allows fungi to deceive innate immune recognition and poses important challenges to control fungal infections. The most promising clinically-relevant treatment against fungal infections is associated with the targeting of the CW biosynthesis, e.g. echinocandins that target β-(1,3)-glucan synthase [10], while nikkomycin Z targets chitin biosynthesis and has been demonstrated to be effective against fungal infection in animal model [11]. Although the chemical composition and the global molecular organization of fungal CWs have been investigated for well-studied species such as *Aspergillus fumigatus* [12], the precise details of the spatiotemporal evolution during CW biosynthesis and how this organelle compensates for the effect of antifungal drugs are still under debate [13,14]. Hoenigl [15]. Analytical approaches based on harsh chemical solubilization using acids or alkali have been used to isolate polysaccharide-rich fractions and analyze them by gas-chromatography coupled with mass spectrometry or solution NMR [16,17] to decipher the chemical nature of fungal CW polysaccharides. However, these semi-destructive approaches are of limited use to understand the native organization of the CW and the structural and dynamic interplay between its different components [18].

In the past decade, solid-state nuclear magnetic resonance spectroscopy, especially performed under magic-angle conditions (MAS NMR), has emerged as a powerful analytical technique to study the molecular organization of CWs in the context of non-solubilized samples. MAS NMR is not limited by the solubility, the crystallinity, the size or the structural homogeneity of the sample. The technique can be applied to biomaterials such as organelles [19], cellular environment [20,21] as well as CWs in prokaryotic or eukaryotic cells [22]. For such samples, MAS NMR techniques present the advantages to be applicable directly on intact cellular preparation obtained directly after culture, without chemical or enzymatic pretreatments that alter the native CW organization.

Pioneered by the group of prof. Mei Hong on plant CWs [23], multi-dimensional ^{13}C-detected MAS NMR techniques, such as two-dimensional (2D) ^{13}C–^{13}C correlation experiments, provides structurally-relevant information to identify the chemical nature of polysaccharides and quantify their molecular abundance within native samples. During the past decade, MAS NMR approaches have been applied to investigate the molecular organization of CWs of various cell types, including fungi [24–26], bacteria[20,27,28], plants [29], algae [30] or on extracted peptidoglycan samples[31–33]. Despite recent commercial release of few ultra-high NMR magnets (>1GHz) and MAS probes allowing very fast spinning frequencies (>100 kHz) and ^{1}H detection, examples of MAS NMR studies using such developments are still extremely scarce [30,34–37,83]. As a consequence, most laboratories working on polysaccharide analysis by MAS NMR usually employ pulse sequences based on direct and indirect ^{13}C detection at moderate MAS frequencies (10–20 kHz). This approach has the advantage to readily give access to ^{13}C polysaccharide chemical shifts, which constitute a highly valuable source of information to identify the chemical nature of the monosaccharide subunits, the branching patterns and the glycosidic linkages [38,18]. As an example, Wang and coworkers recently released a database of MAS NMR ^{13}C chemical shifts to speed up the assignment process [39]. Two 2D experiments are routinely employed to obtain high-resolution correlation spectra and investigate the polysaccharide composition in CWs, i.e. the 2D single-quantum single-quantum (SQ-SQ) dipolar ^{13}C–^{13}C correlation experiment and the 2D double-quantum single-quantum (DQ-SQ) ^{13}C–^{13}C INADEQUATE [40,41]. Their combined use is particularly useful for biological samples containing polysaccharides, due to the relatively poor ^{13}C chemical shift dispersion for carbohydrates and the absence of diagonal peaks in the INADEQUATE experiment. 2D SQ-SQ ^{13}C–^{13}C experiments traditionally used to assign protein ^{13}C resonances have been applied to CW analysis. These pulse sequences include proton-driven spin diffusion (PDSD [42,43], dipolar-assisted rotational resonance (DARR [44] or CORD [45], with examples for cell wall analysis reported by Wang [24,46] and us [25]. These sequences present the key advantage to be applicable at slow and moderate MAS frequencies (~5–20 kHz) [47,48] and, from a spectroscopic point of view, are straightforward to implement on a NMR spectrometer. In 1998, the group of prof. Beat H. Meier introduced the DREAM scheme (for dipolar recoupling enhancement through amplitude modulation) [73,74]. This adiabatic-passage technique employs a radio-frequency (RF) amplitude modulation, with a ^{13}C irradiation matching conditions around half of the MAS frequency to obtain efficient polarization transfers covering a large chemical shift range in proteins [49–51]. The DREAM scheme has several advantages, such as (i) a moderate ^{13}C RF-field strength requirement compared to other recoupling techniques, (ii) efficient polarization transfer and (iii) to be frequency selective at slow-moderate MAS. The DREAM scheme has been implemented in several 2D and 3D pulse sequences used for protein residue assignment, such as ^{15}N-^{13}Cα-^{13}Cβ for intra-residue assignment [50], ^{15}N(^{13}CO)^{13}Cα-^{13}Cβ for sequential assignment or ^{13}C–^{13}C-^{13}C experiments [52–54]. Moreover, Westfeld *et al.* [55] demonstrated that the chemical-shift selectivity of the DREAM scheme could be an advantage to create spectral editing in 2D ^{13}C–^{13}C correlation spectra of amino acids, in order to improve the process of residue resonance assignment.

Inspired by the work of Meier and coworkers on protein samples and small molecules,55], we here investigated the potential of the DREAM scheme to study polysaccharides in the context of the analysis of whole cells. We provide a detailed analysis of the spectral pattern obtained using the DREAM sequence in 2D ^{13}C–^{13}C experiments. We demonstrate that the tuning of the carrier frequency during the DREAM scheme (the pulse sequence is shown in Fig. 1 and Supplementary Fig. 1) could be used to provide a spectral editing and reduce the spectral crowding. Finally, we provide practical considerations for the implementation of the DREAM sequence for whole cell samples.

2. Material and methods

2.1. Sample preparation

Spores of *Neurospora Crassa* (FGSC2489) were spotted on solid Vogel's medium and then incubated for 2 days at 30 °C in dark condition and 2 days at room temperature. Fresh conidia were used to inoculate solid Vogel's medium containing ^{13}C-labeled glucose (15 g/L). Tubes were then incubated for 2 days at 30 °C in dark condition and 2 days at room temperature to promote sporulation. Conidia were collected in milli-Q water by vortexing and filtered through Miracloth® filters. Final conidial suspension was washed in deionized water several times by centrifugation steps (5000 × *g*, 15 min) and the pellet was used to fill in a 4 mm NMR rotor.

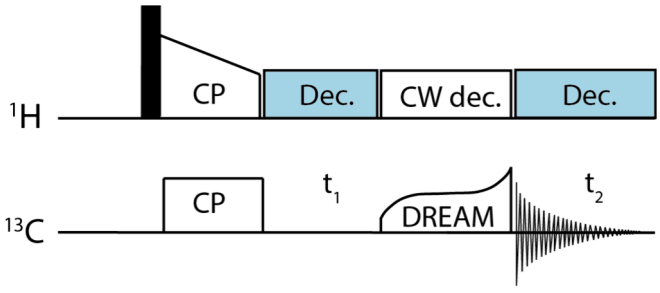

Fig. 1. Pulse scheme of the DREAM experiment used for two-dimensional homonuclear ^{13}C–^{13}C correlation spectroscopy. CP: cross-polarization. Dec: decoupling. CW: continuous wave.

Spores of *Aspergillus fumigatus* (ATCC204305) were harvested from a solid Sabouraud medium by scraping at the surface of the medium immersed in aqueous Tween 0.5 %. Conidia were separated from hyphae by vortexing and filtration through Miracloth® filter. Then, 500 µL of the conidial suspension was inoculated into 100 mL of M9 minimal medium containing U-$^{13}C_6$-glucose (20 g/L) and ^{15}N-labeled ammonium chloride (10 g/L) and incubated for 72 h at 30 °C at 150 rpm. The resulting mycelium was washed with deionized water twice. Then paraformaldehyde (PFA) fixation [56] was performed as follows: the mycelium was incubated for 30 min at room temperature with 2.5 % PFA in PBS with a 1:1 mycelium to buffer ratio (v/v). After discarding the supernatant, the fresh fixation buffer was added, and the suspension was incubated at 4 °C overnight. The next day, residual PFA was quenched with three washes of 0.1 M ammonium chloride and washed twice with deionized water. The pellet was used to pack a 4 mm NMR rotor.

2.2. Solid-state NMR spectroscopy

All experiments were recorded at 600 MHz ^1H frequency (Bruker spectrometer) at 11 kHz MAS using a 4 mm HCN Bruker probe. A cross-polarization contact time of 1 ms and high-power (90 kHz) SPINAL-64 [57] proton decoupling were used. The temperature-dependent position of the water proton resonance was used to set the sample temperature at 5 °C [58].

1D ^{13}C cross-polarization (CP) spectra (Fig. 2) of *N. crassa* and HET-s (218–289) were recorded with respectively 512 and 20 k scans.

2D ^{13}C–^{13}C PDSD spectrum of *N. crassa* was recorded with a mixing time of 50 ms. Acquisition time of 4.5 and 15 ms were used in indirect and direct dimension respectively for a total acquisition time of 10 h.

2D ^{13}C–^{13}C DREAM spectra of *N. crassa* were recorded at various sweep lengths as described in the manuscript. Acquisition time of 4.5 and 15 ms were used in indirect and direct dimension for a total acquisition time of 11 h. An "up" tangential amplitude modulation was used with 1000 discrete steps, centered at 5.5 kHz with a ± 10 % modulation and an estimated homonuclear dipolar coupling of 3640 kHz. During the DREAM sweep, a ^1H continuous wave (CW) decoupling with a field strength of 90 kHz was applied.

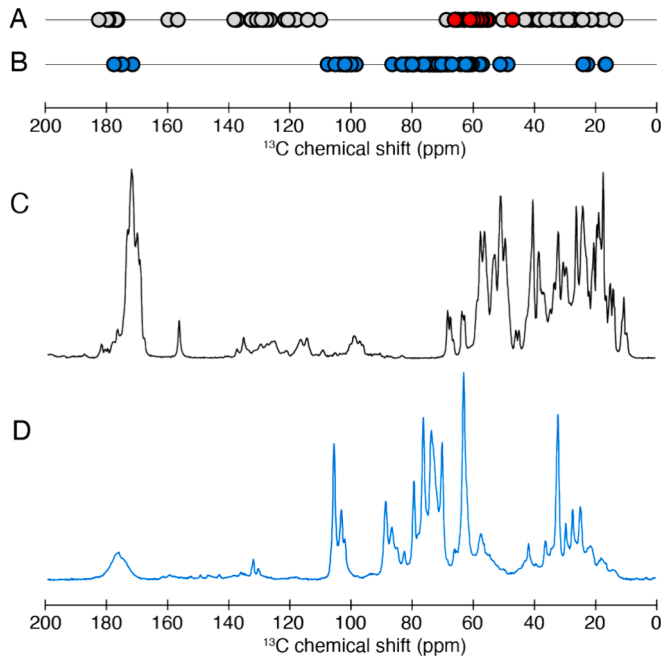

Fig. 2. ^{13}C chemical shift dispersion for amino acids in proteins and polysaccharides. (A) Averaged ^{13}C chemical shifts for all amino acids [82]. Cα's are colored in red. (B) Representative set of ^{13}C chemical shifts for the main polysaccharide units found in plants and fungal microorganisms, extracted from the CCMRD database [39]. (C) ^{13}C cross-polarization spectrum of uniformly ^{13}C-labeled HET-s fibrils (218–289). (D) ^{13}C cross-polarization spectrum of ^{13}C-labeled N. crassa. (For interpretation of the references to colour in this figure legend, the reader is referred to the web version of this article.)

2D ^{13}C–^{13}C PDSD spectrum of *A. fumigatus* was recorded with a mixing time of 50 ms. Acquisition time of 11 and 15 ms were used in indirect and direct dimension respectively for a total acquisition time of 33 h.

2D ^{13}C–^{13}C DREAM spectrum of *A. fumigatus* was recorded with a mixing time of 3 ms. Acquisition time of 11 and 15 ms were used in indirect and direct dimension respectively for a total acquisition time of 33 h. A tangential amplitude modulation was used for the DREAM scheme as described for the *N. crassa* sample.

^{13}C T_1 relaxation times were measured based on an inversion-recovery experiment with a CP excitation. The relaxation times were measured with a delay variation from 0.005 ms to 60 s.

3. Results and discussions

The variety of chemical moieties present in polysaccharides is higher than in side chains of protein amino acids, however their chemical shifts span a similar range. Fig. 2 presents typical ^{13}C chemical shifts found in amino acids, with a distribution that spans between ~ 10 to ~ 185 ppm. Cα chemical shifts (colored in red in Fig. 2A) spans around ~ 55–65 ppm, with the exception of glycine Cα (~47 ppm). As illustrated in Fig. 2C with the 1D ^{13}C CP spectrum of HET-s (218–289) amyloid fibrils, it leads for biosolid proteins to a broad distribution of Cα and side chain signals between ~ 10–68 ppm, a narrow distribution for carbonyl $^{13}C'$ at ~ 178 ppm and few additional signals for aromatic side chains (~110–140 ppm) and Arginine side chain tails (~160 ppm). For polysaccharides found in microbial and plant cell walls, the chemical structure is often composed of 5- or 6-membered carbon heterocycles with oxygen, with a broad variety of side chain groups and branching. This leads to a chemical shift range mainly spanning ~ 55–110 ppm (Fig. 2B and D). In proteins, the DREAM scheme is usually employed to achieve efficient transfer between $^{13}C\alpha$ (~55–65 ppm) and side chain ^{13}C (~10–68 ppm), with a ^{13}C carrier frequency optimized at ~ 50–60 ppm during the DREAM recoupling [54]. We therefore question whether the DREAM scheme, which is a polarization transfer technique that presents a strong dependence on the RF-irradiation frequency at moderate MAS frequencies, might offer spectroscopic advantages compared to broad-band recoupling techniques.

We selected *N. crassa* and *A. fumigatus* as two microbial species to investigate the use of the DREAM scheme to study CW polysaccharides in intact cells. *Neurospora crassa* (Sordariales) is a model organism, which has been at the forefront of fungal biology for more than a century [59]. Playing a crucial role during the early days of molecular biology [60], *N. crassa* has established as a useful model for the exploration of circadian clocks [61], genome defense [62], cell polarity [63], cell fusion [64], allorecognition and regulated cell death[65] and CW composition and biogenesis [66,67]. Like almost all fungi, *N. crassa* relies on a thick CW as a barrier between the fungal cell and the environment, its CW structure and composition have been investigated since the 1950 s [68]. Through a combination of biochemical and genetics analyses, the composition of Neurospora CW has been determined as consisting glucan and chitin [66]. We performed a culture of *N. crassa* in rich medium and fresh conidia were used to inoculate a minimal medium supplemented with ^{13}C-labeled glucose to obtain *N. crassa* conidia uniformly ^{13}C-labeled. Intact conidia were packed into a 4 mm rotor to perform MAS NMR. Fig. 3A presents the 2D ^{13}C–^{13}C PDSD experiment recorded with a mixing time of 50 ms. It reveals three sets of interconnected correlations spanning between ~ 56–108 ppm. The three spin systems were assigned to α-(1,3)glucan, β-(1,3)-glucan and chitin (see Fig. 3B for their chemical structure) based on our previous analysis of fungal CW of intact conidia of *A. fumigatus* [25].

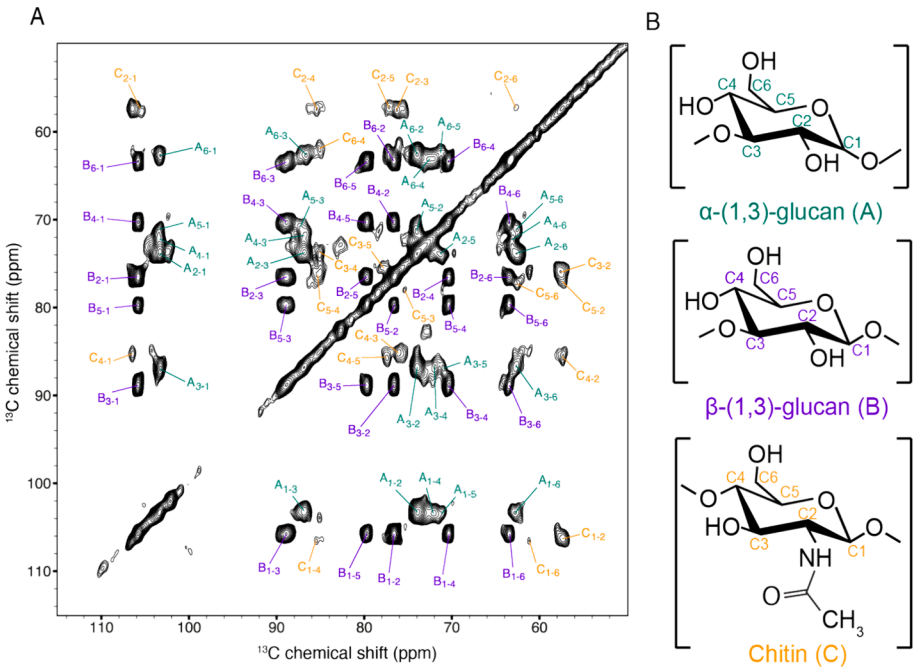

Fig. 3. NMR identification of the main cell wall polysaccharides in intact *N. crassa* conidia. (A) 2D proton-driven spin-diffusion correlation spectrum of *N. crassa*, recorded at 11 kHz MAS at 600 MHz ^{1}H frequency. (B) Chemical structure of α-(1,3)-glucan, β-(1,3)-glucan and chitin.

We implemented a 2D ^{13}C–^{13}C correlation experiment by replacing the PDSD mixing with a DREAM scheme. With initial CP transfers in both experiments, we only excited rigid components of the CW. We used a DREAM sweep duration of 3 ms, to match mixing periods used for proteins (see *vide infra* for its optimization). In analogy to protein samples for which the carrier frequency is set between ^{13}Cα's and sidechain ^{13}C, here we used a carrier frequency at 71 ppm, at the middle of the ^{13}C chemical shifts detected for the three polysaccharides. The resulting 2D DREAM spectrum, exemplified in Fig. 4A for the C_5 correlations of β-(1,3)-glucan (in red and green), presents a distinct spectral pattern compared to the PDSD spectrum (in black). First, we observed a typical pattern of positive-intensity signals at the diagonal (in green in Fig. 4A) and negative-intensity cross-peaks (in red in Fig. 4A), reflecting the double-quantum properties of the DREAM recoupling scheme. In dipolar-based recoupling experiments, the ^{13}C–^{13}C polarization transfer is through-space mediated and correlated to the strength of the dipolar couplings. However, the presence of strong dipolar couplings between covalently attached carbons (e.g. C_5-C_6 and C_5-C_4 if we consider C_5 as the polarization source) can quench smaller dipolar couplings (e.g. C_5-C_1, C_5-C_2 or C_5-C_3) following the so-called "dipolar truncation effect" [69–72]. As a consequence, the resulting polarization pathway could not be simply considered as a sum of direct polarization transfers (Fig. 4B) and possible relayed transfers mediated by one-bond ^{13}C–^{13}C connectivity must be considered (Fig. 4C). In the case of the DREAM scheme performed here with a relatively short mixing period of 3 ms, we observed negative-intensity cross-peaks with strong intensity for one-bond correlation C_5-C_4 and C_5-C_6, and negative-intensity cross-peaks with low intensity for C_5-C_2 and C_5-C_3. Note that the cross-peak encoding for the C_5-C_1 correlation was not observed. This observation reflects that the cross-peaks arise mostly from direct polarization transfers between the correlated carbon nuclei. In addition, the 2D DREAM experiment shows an important asymmetry (full spectrum showed in Supplementary Fig. 2). This effect has already been described [51] and is mainly caused by ^{13}C spin pairs that recouple at different time during the DREAM sweep.

We inspected all possible polarization transfers within the three polysaccharides and found that this trend is not homogeneous. It is exemplified in Fig. 5 for the polarization transfer pathway ending at the C_4 position for the β-(1,3)-glucan. In a model assuming only direct polarization transfers during the DREAM scheme, all correlations associated with C_4 in the direct dimension (i.e. C_1-C_4, C_2-C_4, C_3-C_4, C_5-C_4 and C_6-C_4) should be encoded by negative-intensity cross-peaks. We observed negative cross-peaks for the one-bond ^{13}C–^{13}C correlations C_3-C_4 and C_5-C_4 (Fig. 5A–C). However, the cross-peaks are positive for correlations C_2-C_4 and C_6-C_4. This observation reflects the presence of relayed polarization transfers during the DREAM recoupling. Indeed, in such Cx-Cy-Cz spin systems, a Cx-Cz polarization transfer could be either direct and lead to a negative cross-peak, or be the result of two polarization transfers, first between Cx and Cy (leading to a negative contribution) followed by Cy to Cz (leading to a positive contribution because

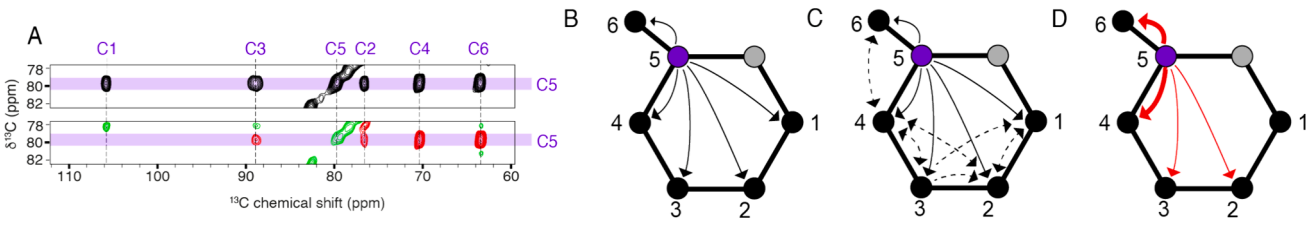

Fig. 4. Polarization transfer pathway in the DREAM experiment. (A) Excerpts of the 2D PDSD spectrum (in black) and DREAM (positive signal in green, negative signal in red) of *N. crassa*. Polarization transfer pathways for the C_5 position of β-(1,3)-glucan (schematically presented), using a PDSD scheme and assuming no relayed contacts (B), assuming relayed contacts (C) and using a DREAM scheme (D). The source polarization (C_5 position of β-(1,3)-glucan) is colored in purple. (For interpretation of the references to colour in this figure legend, the reader is referred to the web version of this article.)

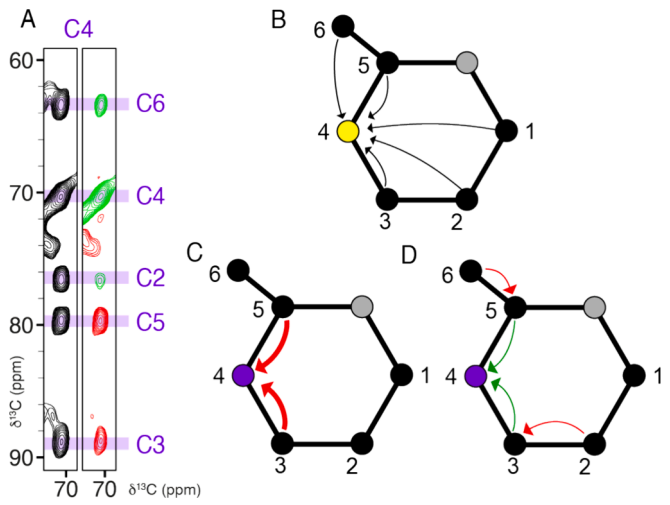

Fig. 5. Polarization transfer pathway and relayed polarization transfer. (A) Excerpts of the 2D PDSD spectrum (in black) and DREAM (positive signal in green, negative signal in red) of *N. crassa*. Polarization transfer pathway ending at the C_4 position of β-(1,3)-glucan, using a PDSD scheme assuming no relayed polarization transfers (B); using a DREAM scheme assuming one-bond transfers (C); and using a DREAM scheme assuming relayed transfers (D). (For interpretation of the references to colour in this figure legend, the reader is referred to the web version of this article.)

of the signal inversion). We therefore hypothesize that the positive cross-peaks encoding C_2-C_4 and C_6-C_4 are the results of relayed transfers as schematized in Fig. 5D. Starting on C_2, the inversion of magnetization will lead to a negative C_2-C_3 cross-peak, followed by a C_3-C_4 polarization transfer leading to a positive C_2-C_4 cross-peak. The same pathway might also explain the positive C_6-C_4 cross-peak. Such Cx-Cy-Cz spin systems exemplified here for glucans are virtually similar to three-spin systems described by Ernst, Böckmann, Meier and coworkers [55] in proteins and named "Cα-Cβ-CX". The main difference between the two spin systems is the chemical shift range, spanning only ~ 25 ppm for glucans and ~ 50 ppm (e.g. for valine Cα-Cβ-$C\gamma_{1/2}$) in proteins. For a microcrystalline Ubiquitin sample, such relayed transfers also led to positive Cα-CX cross-peaks (e.g. Cα-Cγ for Valine), at the expense of direct (and therefore negative) Cα-Cγ transfer [55], depending on the DREAM recoupling conditions. As a side note, the possibility to generate relayed contacts in the 2D ^{13}C–^{13}C DREAM spectra could be envisioned as an advantage during the process of spin system identification. Indeed, the presence of a positive cross-peak would necessarily imply a relayed topology (Cx-Cy-Cz), and as a consequence that the negative-intensity cross-peak encodes for a closer Cx-Cy contact compared to the positive Cx-Cz. It is particularly useful for spin systems observed in polysaccharides compared to their counterparts in amino acids, because several carbohydrates often present a topology made of consecutive and chemically bonded carbons of very close chemical shifts, i.e. C_2, C_3, C_4, C_5 and C_6 in α-(1,3)-glucan and ββ-(1,3)-glucan.

Next, to understand the polarization transfer dynamics during the DREAM scheme, we derived magnetization build-up curves. Fig. 6 presents the build-up curves (Fig. 6A), obtained by varying the sweep duration (from 0.5 to 6 ms), for 4 correlations considering C_4 of β-(1,3)-glucan as the starting polarization source, namely C_4-C_1, C_4-C_2, C_4-C_3 and C_4-C_5 (Fig. 6B). Although such detailed analysis of build-up curves is not available for solid proteins, Verel et al. presented experimental build-up magnetization data on sodium propionate, alanine and zinc acetate [51,73]. Here, we observed that for one-bond ^{13}C–^{13}C contacts (i.e. for C_4-C_5 and C_4-C_3), the optimized sweep duration is ~ 0.5–2 ms. For two-bond (C_4-C_2) and three-bond (C_4-C_1) transfers, we observed slower build-up and a maximum intensity reached respectively at ~ 1 ms and ~ 6 ms. Overall, these optimal durations are shorter compared to those reported for powder and crystalline samples, although the semi-rigidity of the cell wall analyzed here (i.e. ^{13}C T_1 is ~ 3 sec for β-(1,3)-glucan) should be considered. We therefore recommend a DREAM sweep duration of ~ 2–4 ms to analyze CW polysaccharides in whole cells. Note that a detailed analysis of the polarization transfer dynamics, as for instance simulated for canonical amino acids by Meier and coworkers [55] would require extensive numerical simulations, considering that polysaccharide exhibit very strongly dipolar-coupled ^{13}C spin topologies.

The DREAM scheme depends on the frequency of the RF-irradiation (i.e. the ^{13}C carrier position), and the sign of the cross-peaks as well as their intensities are directly dependent on the choice of the ^{13}C carrier position during the DREAM sweep. This effect can be investigated by varying the ^{13}C position used during the DREAM recoupling. For proteins, the carrier position is set at the middle of the recoupled resonances: in 2D ^{13}C–^{13}C DREAM, a carrier position set at ~ 40–45 ppm is typically used [49,50] to cover the full range of Cα's and side chain protein resonances at moderate MAS frequencies, with few exceptions (carbonyls, aromatic side chain and few side chain resonances for Arginine). In the case of a NCαCβ and N(CO)CαCβ experiments, a carrier position set at ~ 55–60 ppm [54] is optimal because the initial ^{13}C polarization transfer before the DREAM is already set to Cα due to the use of a frequency-selective specific ^{15}N-^{13}C CP. For polysaccharides, the chemical shift range differs compared to amino acids. We tested four carrier positions (i.e. at 58, 71.5, 86.5 and 103 ppm) to cover a large part of the ^{13}C resonances of the glucose unit (Fig. 7A). We observed that the four conditions led to four distinct chemical shift patterns (Fig. 7B, C), suggesting a strong dependence of the polarization transfer efficiency to the choice of the carrier position. For a carrier position set to 103 ppm,

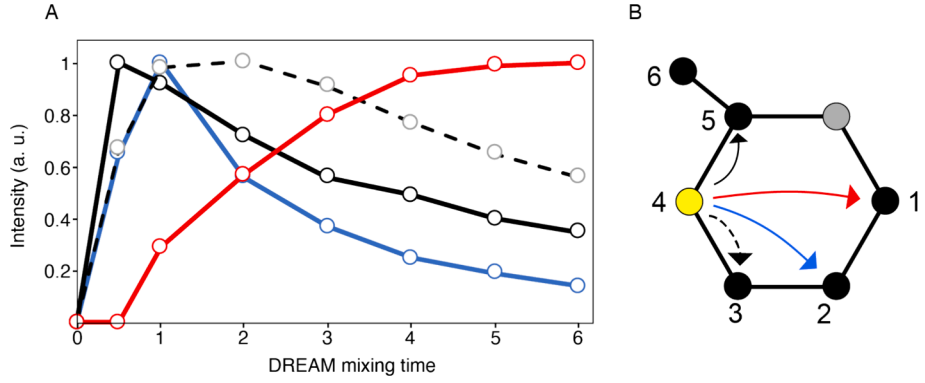

Fig. 6. Polarization transfer dynamics using the DREAM scheme. (A) Build-up magnetization curves for C_4-C_3 (dashed curve), C_4-C_5 (black curve), C_4-C_2 (blue curve), and C_4-C_1 (red curve), correlations. (B) Polarization transfer pathways assuming a direct polarization transfer. (For interpretation of the references to colour in this figure legend, the reader is referred to the web version of this article.)

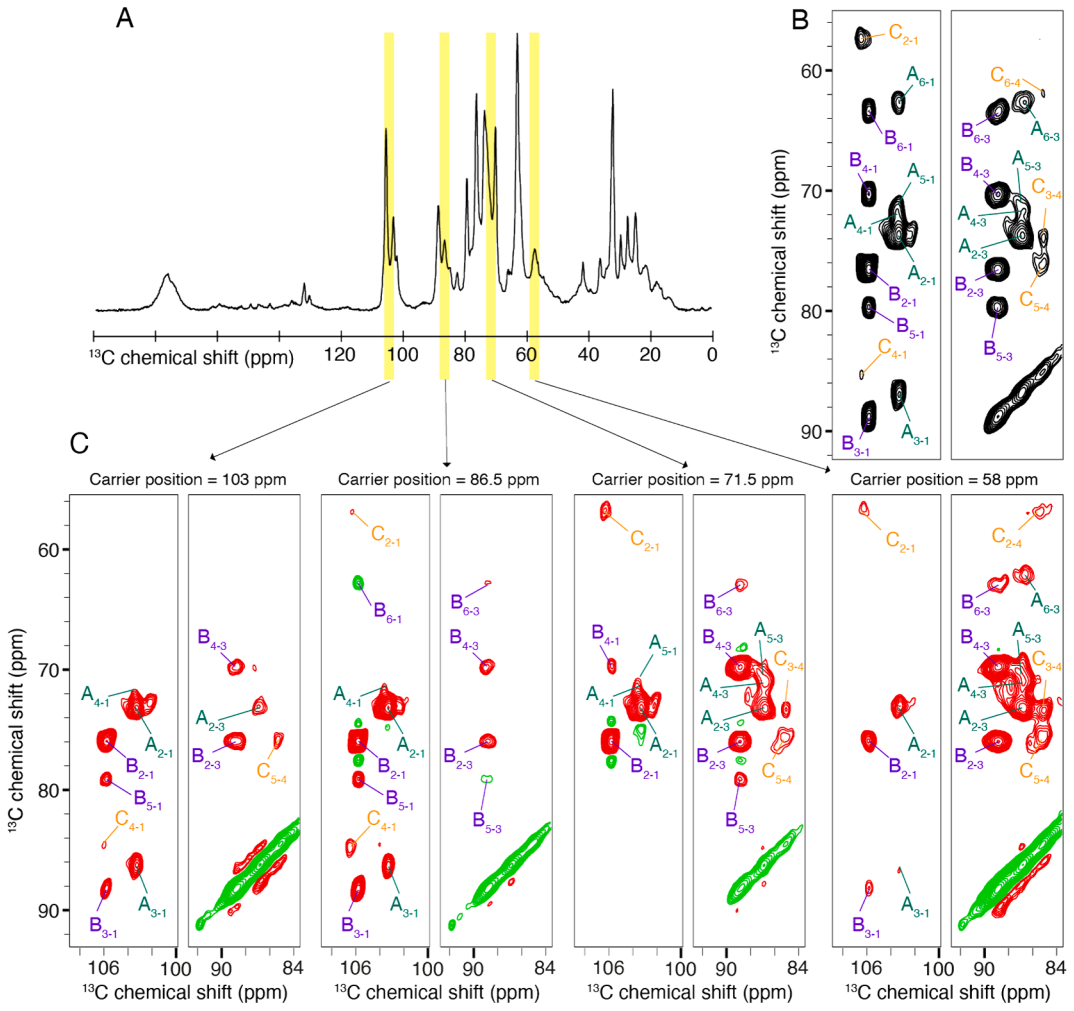

Fig. 7. Spectral editing by varying the carrier position during the DREAM scheme. (A)1D CP spectrum of *N. crassa*. The four ^{13}C carrier positions tested in this study are highlighted in yellow. (B) Excerpt of the 2D ^{13}C–^{13}C PDSD spectrum (α-(1,3)-glucan (green), β-(1,3)-glucan (purple) and chitin (orange)). (C) Excerpt of 2D ^{13}C–^{13}C DREAM spectra obtained for the four carrier positions. (For interpretation of the references to colour in this figure legend, the reader is referred to the web version of this article.)

down-field signals are favorably recoupled (e.g. C_3-C_1 for α- and β-(1,3)-glucan)). Likewise, at a carrier frequency of 58 ppm, up-field signals show strong intensity cross-peaks (e.g. C_6-C_3 for α- and β-(1,3)-glucan)). Overall, a similar effect has been observed in proteins [55], this effect being reinforced in our experimental conditions since the moderate MAS frequency used (11 kHz) is not optimal to cover the full range of chemical shifts. Used in combination with the PDSD experiment (Fig. 7B), the spectral editing provided by the choice of a particular carrier position in the DREAM experiment can be advantageous to intentionally favorize particular spin system topologies according to their chemical shift offsets. Such principle of discriminating spin systems based on their chemical topology was already proposed by R.R. Ernst [74]. For MAS NMR, spectral editing can be achieved through multiple techniques, including depolarization [75], chemical shift filtering [76] or dipolar dephasing [77]. Such approaches have been optimized to provide efficient spectral editing techniques to simplify congested protein spectra [78,79]. In the case of whole cells of *N. crassa*, the efficiency of the spectral editing is noticeable, with several correlations not observed at all carrier positions. A rational understanding of cross-peak intensities as a function of the carrier position is extremely challenging in our case, because the three *N. crassa* CW polysaccharides exhibit strongly dipolar-coupled spin system topologies. As already observed by Meier and coworkers for a microcrystalline protein, the presence of 3- and even 4-carbon multi-spin systems led to complex polarization pathways [55]. Nevertheless, a clear and distinct spectral decongestion of the spectra is observed at various carrier position, facilitating the spectral inspection of such whole cell samples.

Finally, we question whether the results obtained on *N. crassa* could be generalized to other fungal whole cell analysis. We produced a ^{13}C/^{15}N-labeled sample of *A. fumigatus*, an airborne fungal opportunistic pathogen causing invasive aspergillosis [80]. *A. fumigatus* is phylogenetically distant from *N. crassa,* the species have diverged approximately 300 mya, which is comparable to the bird/mammal divergence time [81]. The evolution of the CW architecture during the germination process has been thoroughly scrutinized by MAS NMR methods [25], and CW polysaccharide ^{13}C chemical shift assignments are available [24,25]. We compared 2D ^{13}C–^{13}C correlation experiments obtained using a PDSD mixing (Fig. 8A and C) and a DREAM scheme (Fig. 8B and D). Although the resulting ^{13}C spectral fingerprints differ between the two species due to variable carbohydrate compositional complexity, we observed that the use of the DREAM scheme also enables a spectral editing with the presence of negative- and positive-intensity cross-peaks for *A. fumigatus*.

On the whole, a prototypical set up, based on our results, to achieve an efficient DREAM scheme under moderate MAS would consist of: (1) a MAS frequency at least larger to 7–8 kHz to cover most of the ^{13}C chemical shifts observed in glucose-based carbohydrates, (2) a carrier position around 70–90 ppm to cover a large number of chemical shift

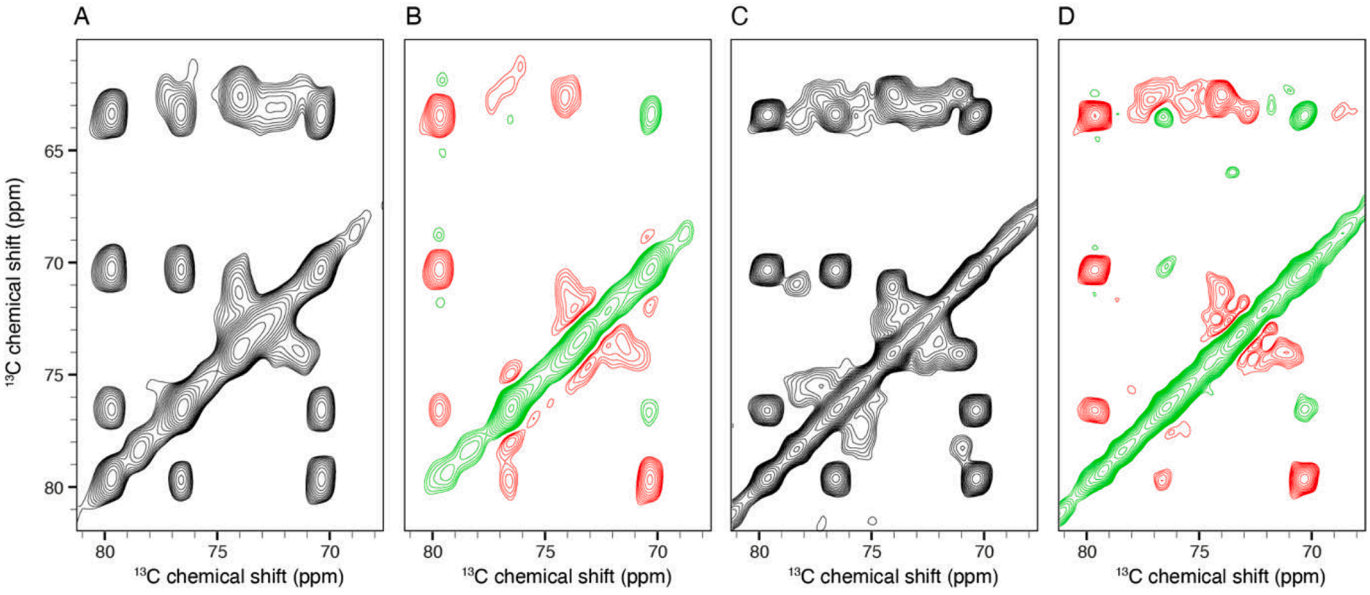

Fig. 8. Excerpts of 2D PDSD spectra of *N. crassa* (A) and *A. fumigatus* (C) and DREAM spectra of *N. crassa* (B) and *A. fumigatus* (D).

offsets and (3) a sweep period of ~ 2 ms. Finally, the recording of a conventional ^{13}C–^{13}C recoupling experiment using either the PDSD, CORD or DARR pulse sequences will provide an optimal set up to compare with the DREAM experiment and (i) distinguish direct to relayed polarization transfers based on the cross-peak sign and (ii) fully exploit the spectral editing provided by the DREAM. To document the practical implementation of the DREAM transfer and optimize spectroscopic parameters such as the carrier position, the choice of the sweep shape and pulse optimization, we present in Fig. 9 the comparison of 1D ^{13}C-detected CP, CP DREAM (i.e. CP followed by a ^{13}C–^{13}C DREAM) and DCP DREAM (i.e. a specific ^{15}N-^{13}C CP followed by a ^{13}C–^{13}C DREAM). While the CP DREAM offers a 1D experiment for which the experimental parameters used in the 2D ^{13}C–^{13}C set up can be directly implemented, it suffers from the complexity of the 1D spectral profile, due to a distorted baseline resulting from the partial superposition of positive and negative signals. We recommend the use of a ^{1}H-^{15}N CP followed by a specific ^{15}N-^{13}C CP prior to the DREAM transfer. In proteins, the 1D NCαCβ DREAM experiment allows to filter out most of the signals due to the specificity of the specific DCP transfer that only selects Cα signals to be transferred during the (Cα-Cβ) DREAM. For polysaccharides, such frequency selectivity based on chemical shift is more challenging to obtain due to the narrower ^{13}C chemical shift distribution. Nevertheless, we achieved a relatively clean 1D spectral profile after the ^{15}N-^{13}C DCP filter (in blue in Fig. 9), and the resulting negative signal at ~ 70–78 ppm (C_3 of chitin) and ~ 106–107 ppm (C_1 of chitin) could be used to monitor and optimize the effect of DREAM parameters such as the sweep pulses. Note that because only chitin contains nitrogen atoms, the sensitivity of the 1D NCC DREAM is lowered by a factor of ~ 15 compared to ^{13}C-detected experiments, due to the low abundance of chitin compared to glucans in *A. fumigatus* [24,25].

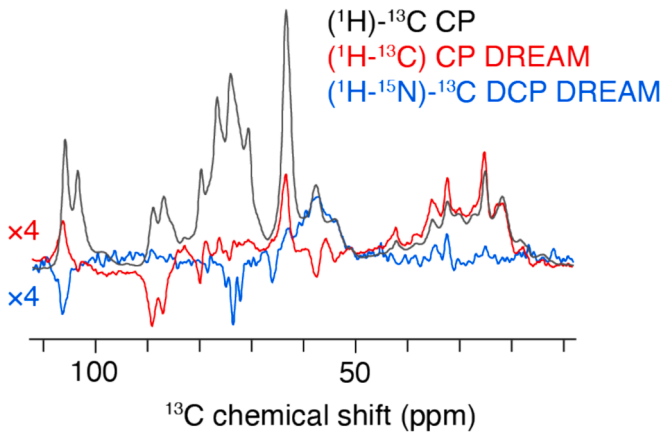

Fig. 9. Optimization of the DREAM scheme for cell wall analysis. 1D spectra obtained on *A. fumigatus*, with (^{1}H)-^{13}C cross-polarization (CP) recorded with 64 scans, (^{1}H–^{13}C)-^{13}C DREAM recorded with 64 scans and (^{1}H-^{15}N-^{13}C) DCP DREAM recorded with 512 scans.

4. Conclusions

We have demonstrated that the DREAM scheme can be implemented to investigate intact whole cell samples. The use two-dimensional ^{13}C–^{13}C correlation experiments employing the DREAM scheme provides selective polarization transfer according to the carbohydrate unit topology. In addition, varying the ^{13}C carrier position during the DREAM sweep provides a spectroscopic tool to access the spectral editing of polysaccharide signals. The DREAM scheme will constitute an additional tool for increasing the repertoire of solid-state NMR techniques to identify and structurally characterize polysaccharides present in cell walls of model and medically-relevant pathogenic microbes. Our results have been obtained under experimental conditions (i.e. medium field NMR magnet, moderate MAS frequency) available to most laboratories working on whole cells analysis by MAS NMR. The study presented here was performed at moderate MAS frequency, and further experiments will be required to investigate how the combination of fast MAS (>60 kHz) and ultra-high magnetic fields could be beneficial to increase the sensitivity and selectivity of the DREAM scheme for CW analysis. By combining MAS NMR and the DREAM scheme, the present study paves the way to develop new approaches to decipher microbial CW at the molecular level, especially to promote the development of CW-targeted antifungals.

Declaration of competing interest

The authors declare that they have no known competing financial interests or personal relationships that could have appeared to influence the work reported in this paper.

Data availability

Data will be made available on request.

Acknowledgments

This work was supported by the ANR TransKingAmyloid (ANR-21-CE11-0007 to A.Lo and S.J.S), the PSGAR-MIE "EMERG" (to L.Delh. and A.Lo) and an ATIP-Avenir funding (to A.D.). This work has benefited from the Biophysical and Structural Chemistry Platform at IECB, CNRS UAR 3033, INSERM US001.

Appendix A. Supplementary data

Supplementary data to this article can be found online at https://doi.org/10.1016/j.ymeth.2024.07.003.

References

[1] M.T. Cabeen, C. Jacobs-Wagner, Bacterial cell shape, Nat. Rev. Microbiol. 3 (2005) 601–610, https://doi.org/10.1038/nrmicro1205.
[2] L.Y.A. Chai, M.G. Netea, A.G. Vonk, B.-J. Kullberg, Fungal strategies for overcoming host innate immune response, Med. Mycol. 47 (2009) 227–236, https://doi.org/10.1080/13693780802209082.
[3] W. Vollmer, Structural variation in the glycan strands of bacterial peptidoglycan, FEMS Microbiol. Rev. 32 (2008) 287–306, https://doi.org/10.1111/j.1574-6976.2007.00088.x.
[4] W.J. Barnes, C.T. Anderson, Release, recycle, rebuild: cell-wall remodeling, autodegradation, and sugar salvage for new wall biosynthesis during plant development, Mol. Plant 11 (2018) 31–46, https://doi.org/10.1016/j.molp.2017.08.011.
[5] N.A.R. Gow, M.D. Lenardon, Architecture of the dynamic fungal cell wall, Nat. Rev. Microbiol. 21 (2023) 248–259, https://doi.org/10.1038/s41579-022-00796-9.
[6] L. Brown, J.M. Wolf, R. Prados-Rosales, A. Casadevall, Through the wall: extracellular vesicles in Gram-positive bacteria, mycobacteria and fungi, Nat. Rev. Microbiol. 13 (2015) 620–630, https://doi.org/10.1038/nrmicro3480.
[7] J. Zhou, Y. Cai, Y. Liu, H. An, K. Deng, M.A. Ashraf, L. Zou, J. Wang, Breaking down the cell wall: Still an attractive antibacterial strategy, Front. Microbiol. 13 (2022) 952633, https://doi.org/10.3389/fmicb.2022.952633.
[8] Y. Zhou, T.B. Reynolds, Innovations in antifungal drug discovery among cell envelope synthesis enzymes through structural insights, J. Fungi Basel Switz. 10 (2024), https://doi.org/10.3390/jof10030171.
[9] J.-P. Latgé, The cell wall: a carbohydrate armour for the fungal cell, Mol. Microbiol. 66 (2007) 279–290, https://doi.org/10.1111/j.1365-2958.2007.05872.x.
[10] W. Hüttel, Echinocandins: structural diversity, biosynthesis, and development of antimycotics, Appl. Microbiol. Biotechnol. 105 (2021) 55–66, https://doi.org/10.1007/s00253-020-11022-y.
[11] T. Chapman, O. Kinsman, J. Houston, Chitin biosynthesis in Candida albicans grown in vitro and in vivo and its inhibition by nikkomycin Z, Antimicrob. Agents Chemother. 36 (1992) 1909–1914, https://doi.org/10.1128/AAC.36.9.1909.
[12] J.-P. Latgé, Cell wall of Aspergillus fumigatus: Variability and response to stress, Fungal Biol. 127 (2023) 1259–1266, https://doi.org/10.1016/j.funbio.2023.05.001.
[13] J.-P. Latgé, T. Wang, Modern biophysics redefines our understanding of fungal cell wall structure, complexity, and dynamics, Mbio 13 (2022) e0114522.
[14] E. Puumala, S. Fallah, N. Robbins, L.E. Cowen, Advancements and challenges in antifungal therapeutic development, Clin. Microbiol. Rev. e0014223 (2024), https://doi.org/10.1128/cmr.00142-23.
[15] Hoenigl Martin, Arastehfar Amir, Arendrup Maiken Cavling, Brüggemann Roger, Carvalho Agostinho, Chiller Tom, Chen Sharon, Egger Matthias, Feys Simon, Gangneux Jean-Pierre, Gold Jeremy A. W., Groll Andreas H., Heylen Jannes, Jenks Jeffrey D., Krause Robert, Lagrou Katrien, Lamoth Frédéric, Prattes Juergen, Sedik Sarah, Wauters Joost, Wiederhold Nathan P., Thompson George R., 2024. Novel antifungals and treatment approaches to tackle resistance and improve outcomes of invasive fungal disease. Clin. Microbiol. Rev. 0, e00074-23. doi: 10.1128/cmr.00074-23.
[16] T. Fontaine, C. Simenel, G. Dubreucq, O. Adam, M. Delepierre, J. Lemoine, C. E. Vorgias, M. Diaquin, J.P. Latgé, Molecular organization of the alkali-insoluble fraction of Aspergillus fumigatus cell wall, J. Biol. Chem. 275 (2000) 27594–27607, https://doi.org/10.1074/jbc.M909975199.
[17] T. Stalhberger, C. Simenel, C. Clavaud, V.G.H. Eijsink, R. Jourdain, M. Delepierre, J.-P. Latgé, L. Breton, T. Fontaine, Chemical organization of the cell wall polysaccharide core of Malassezia restricta, J. Biol. Chem. 289 (2014) 12647–12656, https://doi.org/10.1074/jbc.M113.547034.
[18] J. Duus, C.H. Gotfredsen, K. Bock, Carbohydrate structural determination by NMR spectroscopy: modern methods and limitations, Chem. Rev. 100 (2000) 4589–4614, https://doi.org/10.1021/cr990302n.
[19] S.H. Werby, L. Cegelski, Spectral comparisons of mammalian cells and intact organelles by solid-state NMR, J. Struct. Biol. 206 (2019) 49–54, https://doi.org/10.1016/j.jsb.2018.05.007.
[20] M. Renault, R. Tommassen-van Boxtel, M.P. Bos, J.A. Post, J. Tommassen, M. Baldus, Cellular solid-state nuclear magnetic resonance spectroscopy, Proc. Natl. Acad. Sci. U. S. A. 109 (2012) 4863–4868, https://doi.org/10.1073/pnas.1116478109.
[21] W.N. Costello, Y. Xiao, F. Mentink-Vigier, J. Kragelj, K.K. Frederick, DNP-assisted solid-state NMR enables detection of proteins at nanomolar concentrations in fully protonated cellular milieu, J. Biomol. NMR. (2024), https://doi.org/10.1007/s10858-024-00436-9.
[22] N. Ghassemi, A. Poulhazan, F. Deligey, F. Mentink-Vigier, I. Marcotte, T. Wang, Solid-State NMR Investigations of extracellular matrixes and cell walls of algae, bacteria, fungi, and plants, Chem. Rev. 122 (2022) 10036–10086, https://doi.org/10.1021/acs.chemrev.1c00669.
[23] M. Pérez García, Y. Zhang, J. Hayes, A. Salazar, O.A. Zabotina, M. Hong, Structure and interactions of plant cell-wall polysaccharides by two- and three-dimensional magic-angle-spinning solid-state NMR, Biochemistry 50 (2011) 989–1000, https://doi.org/10.1021/bi101795q.
[24] X. Kang, A. Kirui, A. Muszyński, M.C.D. Widanage, A. Chen, P. Azadi, P. Wang, F. Mentink-Vigier, T. Wang, Molecular architecture of fungal cell walls revealed by solid-state NMR, Nat. Commun. 9 (2018) 2747, https://doi.org/10.1038/s41467-018-05199-0.
[25] G. Lamon, A. Lends, I. Valsecchi, S.S.W. Wong, V. Duprès, F. Lafont, J. Tolchard, C. Schmitt, A. Mallet, A. Grélard, E. Morvan, E.J. Dufourc, B. Habenstein, J. I. Guijarro, V. Aimanianda, A. Loquet, Solid-state NMR molecular snapshots of *Aspergillus fumigatus* cell wall architecture during a conidial morphotype transition, Proc. Natl. Acad. Sci. 120 (2023), https://doi.org/10.1073/pnas.2212003120 e2212003120.
[26] C. Chrissian, E. Camacho, M.S. Fu, R. Prados-Rosales, S. Chatterjee, R.J.B. Cordero, J.K. Lodge, A. Casadevall, R.E. Stark, Melanin deposition in two Cryptococcus species depends on cell-wall composition and flexibility, J. Biol. Chem. 295 (2020) 1815–1828, https://doi.org/10.1074/jbc.RA119.011949.
[27] H. Takahashi, I. Ayala, M. Bardet, G. De Paëpe, J.-P. Simorre, S. Hediger, Solid-state NMR on bacterial cells: selective cell wall signal enhancement and resolution improvement using dynamic nuclear polarization, J. Am. Chem. Soc. 135 (2013) 5105–5110, https://doi.org/10.1021/ja312501d.
[28] X. Liu, J. Brčić, G.H. Cassell, L. Cegelski, CPMAS NMR platform for direct compositional analysis of mycobacterial cell-wall complexes and whole cells, J. Magn. Reson. Open 16–17 (2023) 100127, https://doi.org/10.1016/j.jmro.2023.100127.
[29] T. Wang, P. Phyo, M. Hong, Multidimensional solid-state NMR spectroscopy of plant cell walls, Solid State Nucl. Magn. Reson. 78 (2016) 56–63, https://doi.org/10.1016/j.ssnmr.2016.08.001.
[30] A.A. Arnold, B. Genard, F. Zito, R. Tremblay, D.E. Warschawski, I. Marcotte, Identification of lipid and saccharide constituents of whole microalgal cells by ^{13}C solid-state NMR, Biochim. Biophys. Acta 1848 (2015) 369–377, https://doi.org/10.1016/j.bbamem.2014.07.017.
[31] G. Tong, Y. Pan, H. Dong, R. Pryor, G.E. Wilson, J. Schaefer, Structure and dynamics of pentaglycyl bridges in the cell walls of Staphylococcus aureus by 13C–15N REDOR NMR, Biochemistry 36 (1997) 9859–9866, https://doi.org/10.1021/bi970495d.
[32] T. Kern, S. Hediger, P. Müller, C. Giustini, B. Joris, C. Bougault, W. Vollmer, J.-P. Simorre, Toward the characterization of peptidoglycan structure and protein-peptidoglycan interactions by solid-state NMR spectroscopy, J. Am. Chem. Soc. 130 (2008) 5618–5619, https://doi.org/10.1021/ja7108135.
[33] S.J. Kim, J. Chang, M. Singh, Peptidoglycan architecture of Gram-positive bacteria by solid-state NMR, Biochim. Biophys. Acta 1848 (2015) 350–362, https://doi.org/10.1016/j.bbamem.2014.05.031.
[34] P. Phyo, M. Hong, Fast MAS (1)H-(13)C correlation NMR for structural investigations of plant cell walls, J. Biomol. NMR 73 (2019) 661–674, https://doi.org/10.1007/s10858-019-00277-x.
[35] C. Bougault, I. Ayala, W. Vollmer, J.-P. Simorre, P. Schanda, Studying intact bacterial peptidoglycan by proton-detected NMR spectroscopy at 100 kHz MAS frequency, J. Struct. Biol. 206 (2019) 66–72, https://doi.org/10.1016/j.jsb.2018.07.009.
[36] P. Duan, M. Hong, Selective detection of intermediate-amplitude motion by solid-state NMR, J. Phys. Chem. B 128 (2024) 2293–2303, https://doi.org/10.1021/acs.jpcb.3c06839.
[37] A. Vallet, I. Ayala, B. Perrone, A. Hassan, J.-P. Simorre, C. Bougault, P. Schanda, MAS NMR experiments of corynebacterial cell walls: complementary 1H- and CPMAS CryoProbe-enhanced 13C-detected experiments, J. Magn. Reson. 107708 (2024), https://doi.org/10.1016/j.jmr.2024.107708.
[38] W.A. Bubb, NMR spectroscopy in the study of carbohydrates: characterizing the structural complexity, Concepts Magn. Reson. Part A 19A (2003) 1–19, https://doi.org/10.1002/cmr.a.10080.
[39] X. Kang, W. Zhao, M.C. Dickwella Widanage, A. Kirui, U. Ozdenvar, T. Wang, CCMRD: a solid-state NMR database for complex carbohydrates, J. Biomol. NMR 74 (2020) 239–245, https://doi.org/10.1007/s10858-020-00304-2.
[40] M. Hong, Solid-state dipolar INADEQUATE NMR spectroscopy with a large double-quantum spectral width, J. Magn. Reson. San Diego Calif 1997 (136) (1999) 86–91, https://doi.org/10.1006/jmre.1998.1631.
[41] A. Lesage, C. Auger, S. Caldarelli, L. Emsley, Determination of through-bond carbon−carbon connectivities in solid-state NMR using the INADEQUATE experiment, J. Am. Chem. Soc. 119 (1997) 7867–7868, https://doi.org/10.1021/ja971089k.

[42] N. Bloembergen, On the interaction of nuclear spins in a crystalline lattice, Physica 15 (1949) 386–426, https://doi.org/10.1016/0031-8914(49)90114-7.
[43] N.M. Szeverenyi, M.J. Sullivan, G.E. Maciel, Observation of spin exchange by two-dimensional fourier transform 13C cross polarization-magic-angle spinning, J. Magn. Reson. 1969 (47) (1982) 462–475, https://doi.org/10.1016/0022-2364(82)90213-X.
[44] K. Takegoshi, S. Nakamura, T. Terao, 13C–1H dipolar-assisted rotational resonance in magic-angle spinning NMR, Chem. Phys. Lett. 344 (2001) 631–637, https://doi.org/10.1016/S0009-2614(01)00791-6.
[45] G. Hou, S. Yan, J. Trébosc, J.-P. Amoureux, T. Polenova, Broadband homonuclear correlation spectroscopy driven by combined R2(n)(v) sequences under fast magic angle spinning for NMR structural analysis of organic and biological solids, J. Magn. Reson. San Diego Calif 1997 (232) (2013) 18–30, https://doi.org/10.1016/j.jmr.2013.04.009.
[46] L.D. Fernando, M.C. Dickwella Widanage, S.C. Shekar, F. Mentink-Vigier, P. Wang, S. Wi, T. Wang, Solid-state NMR analysis of unlabeled fungal cell walls from Aspergillus and Candida species, J. Struct. Biol. X 6 (2022) 100070, https://doi.org/10.1016/j.yjsbx.2022.100070.
[47] G. Hou, S. Yan, S. Sun, Y. Han, I.-J.-L. Byeon, J. Ahn, J. Concel, A. Samoson, A. M. Gronenborn, T. Polenova, Spin diffusion driven by R-symmetry sequences: applications to homonuclear correlation spectroscopy in MAS NMR of biological and organic solids, J. Am. Chem. Soc. 133 (2011) 3943–3953, https://doi.org/10.1021/ja108650x.
[48] I. Scholz, M. Huber, T. Manolikas, B.H. Meier, M. Ernst, MIRROR recoupling and its application to spin diffusion under fast magic-angle spinning, Chem. Phys. Lett. 460 (2008) 278–283, https://doi.org/10.1016/j.cplett.2008.05.058.
[49] A. Detken, E.H. Hardy, M. Ernst, M. Kainosho, T. Kawakami, S. Aimoto, B.H. Meier, Methods for sequential resonance assignment in solid, uniformly 13C, 15N labelled peptides: quantification and application to antamanide, J. Biomol. NMR 20 (2001) 203–221, https://doi.org/10.1023/a:1011212100630.
[50] J. Pauli, M. Baldus, B. van Rossum, H. de Groot, H. Oschkinat, Backbone and side-chain 13C and 15N signal assignments of the alpha-spectrin SH3 domain by magic angle spinning solid-state NMR at 17.6 Tesla, Chembiochem. Eur. J. Chem. Biol. 2 (2001) 272–281, https://doi.org/10.1002/1439-7633(20010401)2:4<272::AID-CBIC272>3.0.CO;2-2.
[51] R. Verel, M. Ernst, B.H. Meier, Adiabatic dipolar recoupling in solid-state NMR: the DREAM scheme, J. Magn. Reson. San Diego Calif 1997 (150) (2001) 81–99, https://doi.org/10.1006/jmre.2001.2310.
[52] J. Gath, B. Habenstein, L. Bousset, R. Melki, B.H. Meier, A. Böckmann, Solid-state NMR sequential assignments of α-synuclein, Biomol. NMR Assign. 6 (2012) 51–55, https://doi.org/10.1007/s12104-011-9324-3.
[53] B. Habenstein, C. Wasmer, L. Bousset, Y. Sourigues, A. Schütz, A. Loquet, B. H. Meier, R. Melki, A. Böckmann, Extensive de novo solid-state NMR assignments of the 33 kDa C-terminal domain of the Ure2 prion, J. Biomol. NMR 51 (2011) 235–243, https://doi.org/10.1007/s10858-011-9530-4.
[54] A. Schuetz, C. Wasmer, B. Habenstein, R. Verel, J. Greenwald, R. Riek, A. Böckmann, B.H. Meier, Protocols for the sequential solid-state NMR spectroscopic assignment of a uniformly labeled 25 kDa protein: HET-s(1–227), Chembiochem Eur. J. Chem. Biol. 11 (2010) 1543–1551, https://doi.org/10.1002/cbic.201000124.
[55] T. Westfeld, R. Verel, M. Ernst, A. Böckmann, B.H. Meier, Properties of the DREAM scheme and its optimization for application to proteins, J. Biomol. NMR 53 (2012) 103–112, https://doi.org/10.1007/s10858-012-9627-4.
[56] R. Thavarajah, V.K. Mudimbaimannar, J. Elizabeth, U.K. Rao, K. Ranganathan, Chemical and physical basics of routine formaldehyde fixation, J. Oral Maxillofac. Pathol. JOMFP 16 (2012) 400–405, https://doi.org/10.4103/0973-029X.102496.
[57] B.M. Fung, A.K. Khitrin, K. Ermolaev, An improved broadband decoupling sequence for liquid crystals and solids, J. Magn. Reson. 142 (2000) 97–101, https://doi.org/10.1006/jmre.1999.1896.
[58] A. Böckmann, C. Gardiennet, R. Verel, A. Hunkeler, A. Loquet, G. Pintacuda, L. Emsley, B.H. Meier, A. Lesage, Characterization of different water pools in solid-state NMR protein samples, J. Biomol. NMR 45 (2009) 319–327, https://doi.org/10.1007/s10858-009-9374-3.
[59] R.H. Davis, D.D. Perkins, Timeline: neurospora: a model of model microbes, Nat. Rev. Genet. 3 (2002) 397–403, https://doi.org/10.1038/nrg797.
[60] D.D. Perkins, Neurospora: the organism behind the molecular revolution, Genetics 130 (1992) 687–701, https://doi.org/10.1093/genetics/130.4.687.
[61] C.L. Baker, J.J. Loros, J.C. Dunlap, The circadian clock of Neurospora crassa, FEMS Microbiol. Rev. 36 (2012) 95–110, https://doi.org/10.1111/j.1574-6976.2011.00288.x.
[62] Rountree, M.R., Selker, E.U., 2009. Genome Defense: The Neurospora Paradigm, in: Ferguson-Smith, A.C., Greally, J.M., Martienssen, R.A. (Eds.), Epigenomics. Springer Netherlands, Dordrecht, pp. 321–341. doi: 10.1007/978-1-4020-9187-2_18.
[63] M. Riquelme, O. Yarden, S. Bartnicki-Garcia, B. Bowman, E. Castro-Longoria, S. J. Free, A. Fleissner, M. Freitag, R.R. Lew, R. Mouriño-Pérez, M. Plamann, C. Rasmussen, C. Richthammer, R.W. Roberson, E. Sanchez-Leon, S. Seiler, M. K. Watters, Architecture and development of the Neurospora crassa hypha – a model cell for polarized growth, Fungal Biol. 115 (2011) 446–474, https://doi.org/10.1016/j.funbio.2011.02.008.
[64] A. Fleissner, A.R. Simonin, N.L. Glass, Cell fusion in the filamentous fungus, Neurospora crassa, Methods Mol. Biol. Clifton NJ 475 (2008) 21–38, https://doi.org/10.1007/978-1-59745-250-2_2.
[65] M. Paoletti, Vegetative incompatibility in fungi: From recognition to cell death, whatever does the trick, Fungal Biol. Rev. 30 (2016) 152–162, https://doi.org/10.1016/j.fbr.2016.08.002.
[66] Patel, P.K., Free, S.J., 2019. The Genetics and Biochemistry of Cell Wall Structure and Synthesis in Neurospora crassa, a Model Filamentous Fungus. Front. Microbiol. 10.
[67] J. Verdín, E. Sánchez-León, A.M. Rico-Ramírez, L. Martínez-Núñez, R.A. Fajardo-Somera, M. Riquelme, Off the wall: the rhyme and reason of Neurospora crassa hyphal morphogenesis, Cell Surf. Amst. Neth. 5 (2019) 100020, https://doi.org/10.1016/j.tcsw.2019.100020.
[68] A.J. Shatkin, E.L. Tatum, Electron microscopy of Neurospora crassa mycelia, J. Biophys. Biochem. Cytol. 6 (1959) 423–426, https://doi.org/10.1083/jcb.6.3.423.
[69] A. Grommek, B.H. Meier, M. Ernst, Distance information from proton-driven spin diffusion under MAS, Chem. Phys. Lett. 427 (2006) 404–409, https://doi.org/10.1016/j.cplett.2006.07.005.
[70] P. Hodgkinson, L. Emsley, The accuracy of distance measurements in solid-state NMR, J. Magn. Reson. San Diego Calif 1997 (139) (1999) 46–59, https://doi.org/10.1006/jmre.1999.1759.
[71] M. Hohwy, C.M. Rienstra, R.G. Griffin, Band-selective homonuclear dipolar recoupling in rotating solids, J. Chem. Phys. 117 (2002) 4973–4987, https://doi.org/10.1063/1.1488136.
[72] M.J. Bayro, M. Huber, R. Ramachandran, T.C. Davenport, B.H. Meier, M. Ernst, R. G. Griffin, Dipolar truncation in magic-angle spinning NMR recoupling experiments, J. Chem. Phys. 130 (2009) 114506, https://doi.org/10.1063/1.3089370.
[73] R. Verel, M. Baldus, M. Ernst, B.H. Meier, A homonuclear spin-pair filter for solid-state NMR based on adiabatic-passage techniques, Chem. Phys. Lett. 287 (1998) 421–428, https://doi.org/10.1016/S0009-2614(98)00172-9.
[74] C. Radloff, R.R. Ernst, Spin topology filtration in N.M.R, Mol. Phys. 66 (1989) 161–197, https://doi.org/10.1080/00268978900100091.
[75] X.L. Wu, S.T. Burns, K.W. Zilm, Spectral Editing in CPMAS NMR. Generating subspectra based on proton multiplicities, J. Magn. Reson. A 111 (1994) 29–36, https://doi.org/10.1006/jmra.1994.1222.
[76] J.-D. Mao, K. Schmidt-Rohr, Separation of aromatic-carbon 13C NMR signals from di-oxygenated alkyl bands by a chemical-shift-anisotropy filter, Solid State Nucl. Magn. Reson. 26 (2004) 36–45, https://doi.org/10.1016/j.ssnmr.2003.09.003.
[77] J.-D. Mao, K. Schmidt-Rohr, Recoupled long-range C-H dipolar dephasing in solid-state NMR, and its use for spectral selection of fused aromatic rings, J. Magn. Reson. 162 (2003) 217–227, https://doi.org/10.1016/S1090-7807(03)00012-0.
[78] K. Schmidt-Rohr, K.J. Fritzsching, S.Y. Liao, M. Hong, Spectral editing of two-dimensional magic-angle-spinning solid-state NMR spectra for protein resonance assignment and structure determination, J. Biomol. NMR 54 (2012) 343–353, https://doi.org/10.1007/s10858-012-9676-8.
[79] J.K. Williams, K. Schmidt-Rohr, M. Hong, Aromatic spectral editing techniques for magic-angle-spinning solid-state NMR spectroscopy of uniformly (13)C-labeled proteins, Solid State Nucl. Magn. Reson. 72 (2015) 118–126, https://doi.org/10.1016/j.ssnmr.2015.09.006.
[80] F. Bongomin, S. Gago, R.O. Oladele, D.W. Denning, Global and multi-national prevalence of fungal diseases-estimate precision, J. Fungi Basel Switz. 3 (2017), https://doi.org/10.3390/jof3040057.
[81] X.-X. Shen, J.L. Steenwyk, A.L. LaBella, D.A. Opulente, X. Zhou, J. Kominek, Y. Li, M. Groenewald, C.T. Hittinger, A. Rokas, Genome-scale phylogeny and contrasting modes of genome evolution in the fungal phylum Ascomycota, Sci. Adv. 6 (2020), https://doi.org/10.1126/sciadv.abd0079.
[82] J.C. Hoch, K. Baskaran, H. Burr, J. Chin, H.R. Eghbalnia, T. Fujiwara, M.R. Gryk, T. Iwata, C. Kojima, G. Kurisu, D. Maziuk, Y. Miyanoiri, J.R. Wedell, C. Wilburn, H. Yao, M. Yokochi, Biological magnetic resonance data bank, Nucleic Acids Res. 51 (2023) D368–D376, https://doi.org/10.1093/nar/gkac1050.
[83] A. Safeer, F. Kleijburg, S. Bahri, D. Beriashvili, E.J.A. Veldhuizen, J. van Neer, M. Tegelaar, H. de Cock, H.A.B. Wösten, M. Baldus, Probing cell-surface interactions in fungal cell walls by high-resolution (1) H-detected solid-state NMR spectroscopy, Chem. Weinh. Bergstr. Ger. 29 (2023) e202202616.